Articles

High-Content Screening as a Universal Tool for Fingerprinting of Cytotoxicity of Nanoparticles

Edward Jan, Stephen J. Byrne, Meghan Cuddihy, Anthony M. Davies, Yuri Volkov, Yurii K. Gun'ko, and Nicholas A. Kotov

ACS Nano, **2008**, 2 (5), 928-938 • DOI: 10.1021/nn7004393 • Publication Date (Web): 10 May 2008

ARTICLE

High-Content Screening as a Universal Tool for Fingerprinting of Cytotoxicity of Nanoparticles

Edward Jan,[†] Stephen J. Byrne,[‡] Meghan Cuddihy,[†] Anthony M. Davies,[§] Yuri Volkov,[§] Yurii K. Gun'ko,[‡,*] and Nicholas A. Kotov[†,*]

[†]Departments of Chemical Engineering, Materials Science and Engineering, and Biomedical Engineering, University of Michigan, Ann Arbor, Michigan 48109, [‡]School of Chemistry, Trinity College Dublin, Dublin 2, Ireland, and [§]Department of Clinical Medicine, Trinity College Dublin, Dublin 2, Ireland

ABSTRACT Recent advances and progress in nanobiotechnology have demonstrated many nanoparticles (NPs) as potential and novel drug delivery vehicles, therapeutic agents, and contrast agents and luminescent biological labels for bioimaging. The emergence of new biomedical applications based on NPs signifies the need to understand, compare, and manage their cytotoxicity. In this study, we demonstrated the use of high-content screening assay (HCA) as a universal tool to probe the cytotoxicity of NPs and specifically cadmium telluride quantum dots (CdTe QDs) and gold NPs (Au NPs) in NG108-15 murine neuroblastoma cells and HepG2 human hepatocellular carcinoma cells. Neural cells represent special interest for NP-induced cytotoxicity because the optical and electrical functionalities of materials necessary for neural imaging and interfacing are matched well with the properties of many NPs. In addition, the cellular morphology of neurons is particularly suitable for automated high content screening. HepG2 cells represent a good model for high content screening studies since they are commonly used as a surrogate for human hepatocytes in pharmaceutical studies. We found the CdTe QDs to induce primarily apoptotic response in a time- and dosage-dependent manner and produce different toxicological profiles and responses in undifferentiated and differentiated neural cells. Au NPs were found to inhibit the proliferation and intracellular calcium release of HepG2 cells.

KEYWORDS: nanoparticles · nanomedicine · nanotoxicity · biocompatibility · quantum dots · high content assay · high content screening

Research on nanoparticles (NPs) has generated numerous biological applications in the past decade. With continuing progress of nanoscale synthesis and biological applications of NPs, one needs to develop a quick and fairly standard assessment tool to evaluate their cytotoxicity. Since many structural and physical properties of NPs have clear similarities with those of proteins,[1–3] it is not surprising that NPs may exhibit cytotoxicity or, in more general terms, biological activity that is specific to NPs and affects the cell signaling mechanism differently from that observed for ionic, polymeric systems and small molecules. The detrimental effects of such biological activity can be captured by the term nanotoxicity,[4–6] which is probably the most critical from a health safety perspective.[7]

The purpose of this study is to make the first step toward the development both a fast and fairly comprehensive method of screening of biological activity and cytotoxicity of NPs. We see two important factors that necessitate the development of such protocol(s). (1) Since the synthesis of NPs is much simpler than the synthesis of proteins and other drugs, minor changes in the synthetic protocol are likely to affect their interactions with cells. So, one can expect to see a tremendous surge of potential candidates for toxicity/biological activity screening. Taking II−VI semiconductor quantum dots (QDs) as an example, beside the release of heavy metal elements from the core which can lead to cell poisoning,[8] studies have shown that the cytotoxicity of these QDs is highly dependent on their processing parameters[9] and surface modifications[8–10] as well as a number of physicochemical and environmental factors, such as size, charge, concentration, and stability.[11] Such amounts will be difficult to analyze using conventional approaches. (2) Considering the diversity of NPs being synthesized, one needs a unified approach for screening nanomaterials. Such a systematic approach is not only fundamental to the construction of a unified database for biological and cytotoxic effects of nanomaterials but will also enable scientists to synthesize safer and more efficacious nanostructures at an ever-more efficient rate. We can expect the engineering of biologically functional nanostructures to follow the path of synthetic pharmaceuticals in drug discovery. In the near future, panels of NPs with slightly varying properties and structures will be synthesized and evaluated for cytotoxicity before qualified candidates are designated subsequent developments.

*Address correspondence to igounko@tcd.ie, kotov@umich.edu.

Received for review December 21, 2007 and accepted March 31, 2008.

Published online May 10, 2008.
10.1021/nn7004393 CCC: $40.75

In this study, we are motivated to explore the possibility of building a high-content, high-throughput cytotoxicity assay platform based on high-content screening (HCS) technology to meet the future's demand for nanotoxicity studies. HCS is a recent advance in the integration and automation of quantitative fluorescence microscopy and image analysis, and it has already started to generate impact in pharmaceutical and biotechnology industries.[12,13] Zhang *et al*. were the first to employ high-content image analysis, in conjunction with high-throughput analysis, to study the cytotoxicity of QDs.[14] They investigated the cellular and molecular effect of high doses of poly(ethylene glycol) silanized QDs (PEG-silane-QDs) on human lung and skin epithelial cells and reported PEG-silane-QDs to induce minimal cytotoxicity even at high dosages. While the use of HCS analysis in their study is confined to cell counting, quantification of apoptotic and necrotic cell population, and generation of cell cycle profiles, our current study extends the application of HCS technology to the evaluation of cell function, specifically neurite outgrowth, and the development of a multiplexed cytotoxicity assay that may serve as the basis of a standardized nanotoxicity assay and facilitate the formation of a unified nanotoxicology database.

Our study begins with a comprehensive investigation of cadmium telluride (CdTe) QD induced cytotoxicity in NG108−15 murine neuroblastoma cells using various HCS assays. We then extend the application of our multiplexed cytotoxicity assay to study the cytotoxic effect of gold (Au) NPs (NPs) on the HepG2 human hepatocellular carcinoma cells. Semiconductor QDs are most well-known for their potential applications in biosensing, *ex vivo* live-cell imaging and *in vivo* animal targeting,[15−18] while Au NPs have demonstrated promising capabilities as novel drug delivery vehicles,[19] near-infrared agents for thermal therapy,[20] and contrast agents for biomedical imaging.[21−23] More recently in search of new neurotherapeutic, neuroprosthetic, and neuroimaging strategies, many researchers have explored the use of NPs to manipulate and create active cellular interfaces with nerve cells.[24,25] Vu *et al*. utilized peptide conjugated QDs to initiate neuronal differentiation[26] while Dahan *et al*. used antibody functionalized QDs to track the diffusion of glycine receptors in neurons.[27] Jackson and colleagues demonstrated that QDs can improve identification and visualization of brain tumors.[28] At the neural interface, Winter *et al*. investigated the possibility to build a bioelectronic interface by both culturing nerve cells on tethered QD thin films[29] and attaching QDs directly to nerve cells *via* biological recognition molecules.[30] Most recently, Kotov and colleagues demonstrated, for the first time, the excitation of neural cells through a sequence of photochemical and charge-transfer reactions on layer-by-layer assembled NP-polyelectrolyte composite films.[31]

RESULTS AND DISCUSSION

CdTe Quantum Dots. One question we would like to answer in our exploration of HCS technology and assays is how undifferentiated and differentiated cells respond to treatment with NPs. This is an important question because target cells at various stages of differentiation and maturation respond to therapeutic interventions in different ways. To answer this, we investigated the cellular response of the NG108-15 murine neuroblastoma cells to two types of CdTe QDs. The first is a thioglycolic acid (TGA)-capped CdTe QD (TGA-QD), and the other is a TGA-capped CdTe QD produced in the presence of gelatin (Gelatin-QD). Both of these QDs have a diameter of 3 nm and emit in the green-yellow region of the spectrum (~560 nm). Some of us recently published the synthesis and characterization of this Gelatin-NP nanocomposite along with a preliminary cytotoxicity study that demonstrated reduced cytotoxicity of Gelatin-QDs in THP-1 human monocytic cells.[32] It has been suggested that gelatin enables the QDs to grow more discretely (blue-shifted) and serves as a co-capping agent for stabilization of QDs and encapsulation of the toxic heavy metal core. While poly(ethylene glycol) (PEG) remains the most promising coating material for reducing cytotoxicity to this date, we believe naturally occurring biopolymers, such as gelatin, may provide additional biological functionalities in addition to their protective property. We chose to work with the NG108-15 murine neuroblastoma cells because they possess neuron-like properties and can be differentiated relatively easily and quickly.

The first HCS assay we employed was an apoptosis/necrosis assay for the quantification of healthy, apoptotic, and necrotic cells. At the indicated time point (1.5 h, 6 h, 24 h) following treatment with TGA-QDs or Gelatin-QDs, cells were stained with propidium iodide (1 μg/ml) and Hoechst 33342 (2 μg/ml) for 10 min at room temperature and imaged using the IN Cell Analyzer 1000 HCS system (GE Healthcare). Cells in each category were classified using the supervised classification function of the IN Cell Investigator image analysis software (GE Healthcare), which analyzed the fluorescence quantitatively on a cell-by-cell basis. Figure 1 illustrates representative images of healthy, apoptotic, and necrotic cells. The plasma membranes of necrotic cells are permeable to propidium iodide, so necrotic cells were identified by their intense red fluorescence. Apoptotic cells were identified as being impermeable to propidium iodide but showing condensed and fragmented nuclei from the Hoechst 33342 stain. Healthy cells were stained by Hoechst 33342 only and displayed intact and homogeneously stained nuclei. The experiment was carried out in triplicates in 96-well plates, which helps to increase throughput and reduce consumption of cell culture and assay reagents and ensures reproducibility at the large cell population scale.

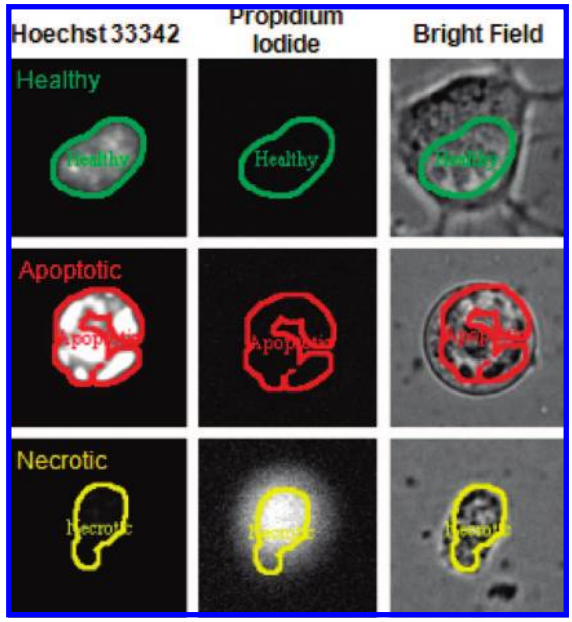

Figure 1. Representative fluorescence and bright field images of a healthy (green outline), an apoptotic (red outline), and a necrotic (yellow outline) cell. Cells were stained simultaneously with Hoechst 33342 (blue channel, first column) and propidium iodide (red channel, middle column). Outline and classification of cells were generated by the IN Cell Investigator image analysis software using the supervised classification capability.

Figure 2 shows the average result from three independent runs. For each run, five independent fields from each well were imaged using a 20× objective. The entire experiment, including all concentrations and time points, is an assessment of as many as 25 000 individually analyzed cells and demonstrates the robustness of HCS assays. For both undifferentiated and differentiated cells, treatment with QDs induced predominantly an increase in apoptotic cell population, as the number of necrotic cells remained relatively constant regardless of QD dosage or treatment time. This finding is corroborated by published results from Chan *et al.*, who demonstrated that CdSe-core QDs induce apoptotic biochemical changes in human neuroblastoma cells *via* mitochondrial-dependent pathways and inhibition of survival signals.[33] In addition, our study also found undifferentiated and differentiated cells to respond differently to treatment with QDs. This is an important finding because the human is composed of cells and tissue at different levels of maturity and differentiation. For undifferentiated NG108-15 cells, the number of apoptotic cells remained constant between 1.5 and 6 h of incubation with QDs and increased sharply after 24 h. We suspect the delayed cytotoxic response is a buffering effect owing to the proliferating potential and innate properties of undifferentiated cells. For differentiated cells, an incremental increase in apoptotic population was observed between the three time points, indicating differentiated cells to be more sensitive to QD treatment.

It should be emphasized that although TGA-QDs and Gelatin-QDs produced similar cellular response in NG108-15 cells, in HCS assays even a 5−15% difference represents a consistent and significant response at the cell population level and is likely to include moderate and below average response typical of the *in vivo* physi-

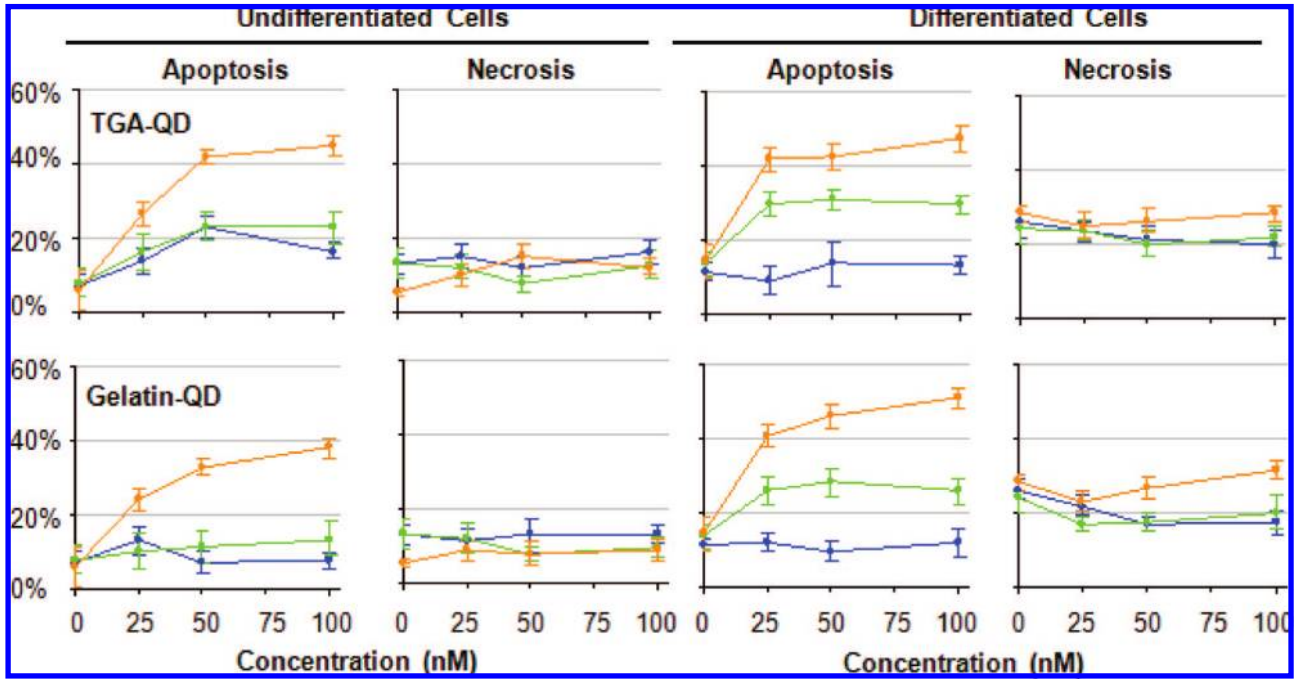

Figure 2. Effect of QD treatment on NG108-15 cells. Undifferentiated and differentiated NG108-15 cells were incubated with various concentrations of TGA-QDs and Gelatin-QDs for 1.5 (blue), 6 (green), and 24 h (orange). Percentages of apoptosis and necrosis at the indicated time points were determined by staining the cells with propidium iodide and Hoechst 33342, followed by image acquisition and analysis using a HCS system.

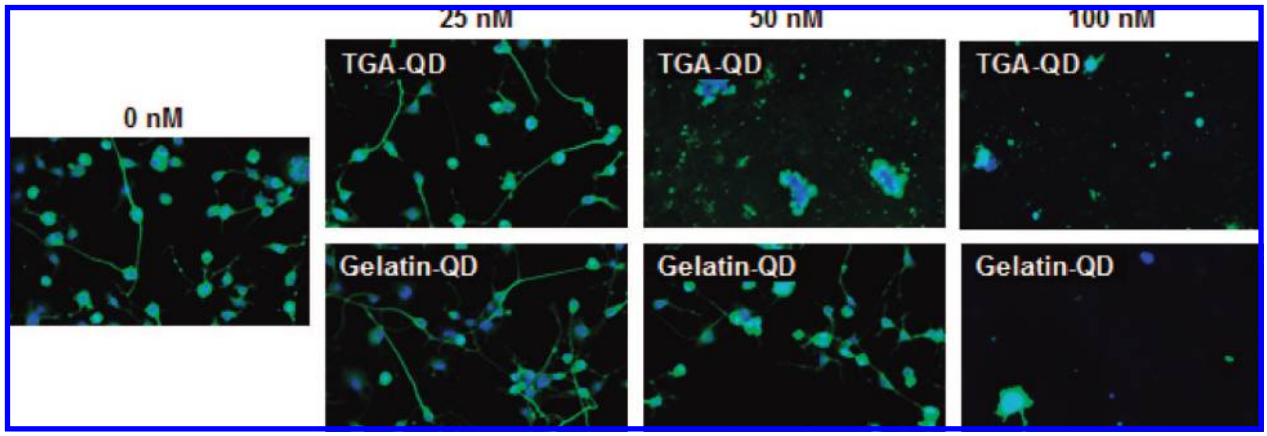

Figure 3. Effect of QD treatment on neurite outgrowth of NG108-15 cells. Cell were incubated with TGA-QDs and Gelatin-QDs at various concentrations for 6 h and induced to differentiate for 4 additional days in low-serum medium. Cells were stained for β-tubulin III (green) and nuclei (blue) and imaged using a HCS system.

ological situations. The most obvious difference between the two QDs is seen in the apoptotic population of the undifferentiated cells. While the apoptotic population of TGA-QD treated cells increased with QD concentration at 1.5 and 6 h, the apoptotic population of Gelatin-QD treated cells remained unchanged. In addition, TGA-QD treated cells also displayed a more drastic increase in apoptotic population after 24 h compared to Gelatin-QD treated cells, indicating somewhat lower cytotoxicity in the Gelatin-QDs. Generalizing the results, it is important to make three points here. (1) HCS allows one to reliably identify these differences in cellular response to NPs and use it for comparison of their (bio)medical prospects, which provides a substantial advantage over less systematic techniques used now. (2) We used here a version of analysis with a fairly wide concentration step, and finer profiles could be obtained to highlight even smaller effects for more advanced fingerprinting. (3) A greater number of labels in the panel will further improve differentiation of the effect of one NPs *versus* the other or one cell type *versus* the other, which will be demonstrated below.

To further investigate the difference between TGA-QDs and Gelatin-QDs, we conducted a neurite outgrowth assay to investigate the effect of QD pretreatment on neuronal differentiation. One day following cell seeding, NG108-15 cells were incubated with either type of QDs for 6 h, after which the cells were washed with fresh medium and cultured in medium with reduced amount of serum to induce differentiation. No supplementary growth factor was added in order to avoid interference or counteracting effect. After four days of differentiation, cells were stained and imaged using the IN Cell Analyzer 1000 HCS system. Cells were first fixed in 2% paraformaldehyde and permeabilized in 0.1% Triton X-100 in 1% BSA. Neurites were stained using mouse anti-β-tubulin III (1:800 in 1% BSA; overnight at 4 °C) followed by Alexa Fluor 488 conjugated goat antimouse IgG (1:200; 1 h at 37 °C). The experiment was carried out in triplicate. For each well, four independent fields were imaged using a 10× objective and analyzed using the IN Cell Investigator software.

Figure 3 shows representative images acquired by the robotic imaging system at different treatment conditions. The measurement of neurite outgrowth is traditionally a time-consuming and tedious job, but the work is greatly simplified with the aid of a HCS system. An analysis of the total neurite length with respect to the untreated control is presented in Figure 4. A 6 h treatment with 25nM of TGA-QDs prior to neuronal differentiation reduced the total neurite length by approximately 50%, primarily due to a decrease in cell number as illustrated in Figure 3. However, treatment with 25 nM of Gelatin-QDs led to a slight increase in total neurite length. We suspect this contradicting effect at low dose could be a hormetic response as hormesis is frequently observed as a result of low-dose stimulation in toxicological studies.[34,35] The mechanisms involved in countering the cytotoxic effect of a short, nonlethal low-dose treatment might have stimulated the formation of neurites. The difference between the two QDs is most evident at the 50 nM concentration, where all TGA-QD treated cells were killed while Gelatin-QD treated cells still exhibited some viability and a moderate level of neurite outgrowth. A 100 nM treatment with either type of QDs appeared to be too toxic for any cells to survive.

The apoptosis/necrosis assay and neurite outgrowth assay prompted us to further investigate the cellular response of neural cells to QD treatments. The apoptosis/necrosis assay measures only late-stage toxicity and cellular events associated with a lethal apoptotic or necrotic effect. This assay is important but needs to be augmented with other assays for detailed toxicology fingerprinting, because it provides little mechanistic understanding of toxicological effects. The neurite outgrowth assay clearly revealed the toxicological difference between the two QDs and demonstrated the importance of a functionality assay in cytotoxicity stud-

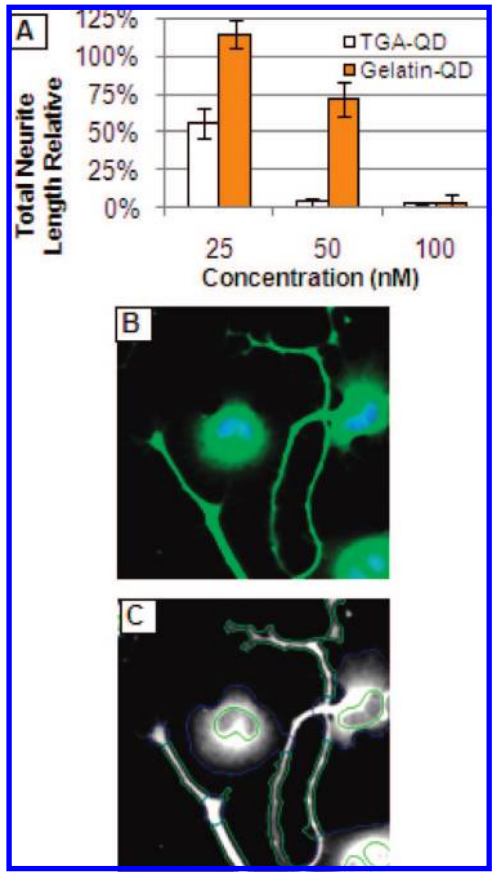

Figure 4. Neurite outgrowth was assessed in terms of total neurite length per field. The result is the average of three independent experiments (four independent fields each) and is expressed as percentage relative to the total neurite length per field of the untreated control (A). A false-colored composite fluorescent image of neurite outgrowth is shown here (B). During image analysis, the software's image processing algorithm allows the system to identify neurites (green outlines) and make quantitative measurements (C).

ies. Since our motivation is to explore the use of HCS assays for the study of nanotoxicity, we subsequently employed another kind of assay, this time an assay that would detect sublethal cytotoxicity in a multiparameter format to give us more information and sensitivity regarding the cytotoxicity of a given nanocolloid.

Although the success and advantages of a sublethal, multiplexed cytotoxicty assay have been demonstrated by O'Brien and his colleagues in the study of hepatotoxicity,[35,36] it has never been utilized in the context of nanotoxicity. Such an assay evaluates specific toxicological mechanisms in cells prior to the onset of the late stages of nonspecific degeneration and apoptotic or necrotic death, providing greater predictive power and extrapolatability across models and species.[36] The multiparametric nature of the assay originates from the multiple fluorescent probes that simultaneously and coherently monitor different cellular functions *in vitro* and is made possible by recent advances in fluorescent probe technology.[37]

In this study, undifferentiated and differentiated NG108-15 cells were treated with QDs at various concentrations for 24 h, after which the medium was removed and the cells were incubated with a cocktail of fluorescent probes for 30 min before they were imaged using the IN Cell Analyzer 1000 HCS system. The cocktail of fluorescent probes was prepared in fresh medium and consisted of 1 μM Hoechst 33342, 20 nM TMRM, and 1 μM Fluo-4. These fluorescent probes were selected for specific reasons. First of all, these fluorescent probes can be used concurrently and are readily internalized by live cells without posing substantial harm. Hoechst 33342 allows identification of individual cell nuclei, which permits the measurement of cell count and nuclear area and allows subsequent analysis on the complementary stains to be conducted. A decrease in cell number indicates cell death and/or decreased cell proliferation, while nuclear shrinkage is typically a consequence of chromatin condensation and a sign of apoptotic cell death. TMRM and Fluo-4 allow the assessment of mitochondrial membrane potential and intracellular free calcium concentration, respectively. The mitochondrion is central to the functioning and survival of nerve cells.[38] It is responsible for ATP generation, Ca^{2+} uptake and storage, and the generation of detoxification of reactive oxygen species.[39] A drop in the electrochemical gradient across the mitochondrial membrane therefore signals weakened cellular respiratory capacity and energetics. Intracellular Ca^{2+} is a chief regulator of a variety of biological processes.[40] For this reason, pharmaceutical companies have long adopted the measurement of intracellular Ca^{2+} for high-throughput screening.[41] Intracellular Ca^{2+} is especially important in neural cells since it regulates neurite outgrowth and synaptogenesis, synaptic transmission and plasticity, and cell survival.[42,43] A dramatic increase in intracellular Ca^{2+} is an early event in the development of cell injury due to cytotoxicity.[44]

The concentration−response of cells was measured using the IN Cell Investigator software and evaluated in terms of cell number, nuclear area, mitochondrial function, and intracellular calcium homeostatsis. Cell count was generated from the number of Hoechst 33342 stained nuclei. Nuclear size was defined as the area of Hoechst 33342 fluorescence (Figure 5, inner blue circle). Cellular mitochondrial membrane potential was defined as the TMRM fluorescence intensity in punctuate cytosolic regions around the nucleus (Figure 5, yellow inclusions), while intracellular free calcium concentration was measured by the fluorescence intensity of Fluo-4 in a large intracellular circular region centered at the nucleus (Figure 5, outer green circle). Since the HCS platform is based on the acquisition, processing, and analysis of fluorescence images, we made sure the NG108-15 cells do not uptake a significant amount of QDs to interfere with our multiplexed cytotoxicity assay (data not included). The level of fluorescence signal from QDs was constant regardless of concentration and was well below the basal fluorescence level of

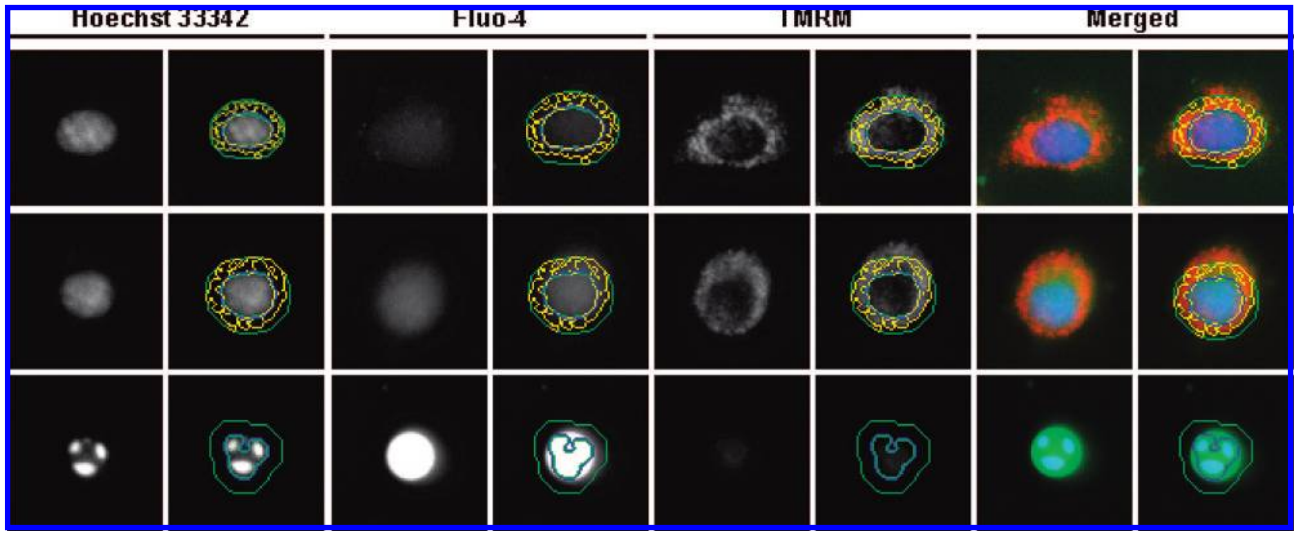

Figure 5. Representative fluorescence images of a healthy (first row), an impaired (middle row), and a dying (last row) cell acquired and processed by the IN Cell HCS system. The nucleus, stained by Hoechst 3342, is outlined by a blue circle. The cell body or the intracellular region is enclosed by a green circle, within which the intensity of Fluo-4 fluorescence is measured. The punctuate, TMRM-bound mitochondrial organelles in the cytosol are identified by the yellow inclusions. In the merged images, Hoechst 3342, Fluo-4, and TMRM stains are shown in blue, green, and red, respectively. As the health condition of cells deteriorates, the nucleus shrinks and becomes fragmented, the Fluo-4 stain intensifies and signals a sharp increase in intracellular free calcium concentration, and the TMRM stain diminishes as a result of reduction in mitochondrial membrane potential.

TMRM and Fluo-4. This was not a problem in the apoptosis/necrosis and neurite outgrowth assays because the emission spectrum of the QDs does not coincide with Hoechst 33342 and propidium iodide and immunological staining is much more specific and intense than nonspecific uptake and adsorption of the QDs.

Figure 6 shows the average result of our multiplexed cytotoxicity fingerprinting. Overall, cell count appears to be the most sensitive indicator of cytotoxicity, as significant changes in cell count tend to occur at a much lower QD concentration than the other parameters. In addition, the largest difference between the toxicity profiles of TGA-QD- and Gelatin-QD-treated cells is observed in this fluorescence parameter. For Gelatin-QD- and TGA-QD-treated cells, the cell count falls below 70% at 12.5 and 1.56 nM, respectively, in undifferentiated cells and at 1.56 and 0.39 nM, respectively, in differentiated cells. Similar findings are observed in the other parameters, where the onset of change in the parameters consistently occurs at a lower QD concentration in TGA-QD treated cells and in differentiated cells. These differences are summarized in Table 1 and have two implications. (1) It is confirmed that the Gelatin-QDs are less cytotoxic and more biocompatible than the TGA-QDs although the cytotoxic effects of Gelatin-QDs are still substantial. The gelatin-CdTe nanocomposite reduced the sublethal concentration (>30% cell death) of CdTe QDs by at least 4 times in both undifferentiated and differentiated cells (Table 1). This outcome validates our rationale behind the incorporation of biological molecules in the synthesis of NPs as a means to achieve better stability and biocompatibility. We have to keep in mind that the toxic effect of CdTe made in a general synthetic route described here can never be eliminated but modified or reduced, and we use these NPs here as a model system. We also have to reiterate that although some of the observed differences between the two QDs could potentially be interpreted as marginal, the fact is that in systems implementing HCS principles a 5−15% difference represents a consistent and significant response because of the large cell population being analyzed. The close resemblance between the toxicity profiles of TGA-QDs and Gelatin-QDs also indicates that their toxicities share a common source, which most likely comes from the leakage of cadmium from the core of the NPs. (2) Already indicated by the apoptosis/necrosis assay is that differentiated cells are more sensitive and vulnerable to QD-induced cytotoxicity, which correlates with the fact that they are generally regarded as more sensitive to the environment. The large number of fragmented nuclei (Figure 5, last row) observed at high QD concentrations again confirms apoptosis as the primary cellular response to the QD-induced cytotoxicity. Besides the larger scale of decrease in cell count and mitochondrial membrane potential observed in differentiated cells, the hormetic response in the nuclear area observed in undifferentiated cells is absent in differentiated cells and is replaced by marginal reduction. While the mitochondrial membrane potential of undifferentiated cells follows an inverse decay, the same parameter appears to decay exponentially in differentiated cells and could possibly explain their vulnerability to QD-induced apoptosis. We suspect these differences in cellular response arise from changes in biological machinery as cells differentiate.[45] Changes involving mitochondria, membrane structures, and protein modifications may ac-

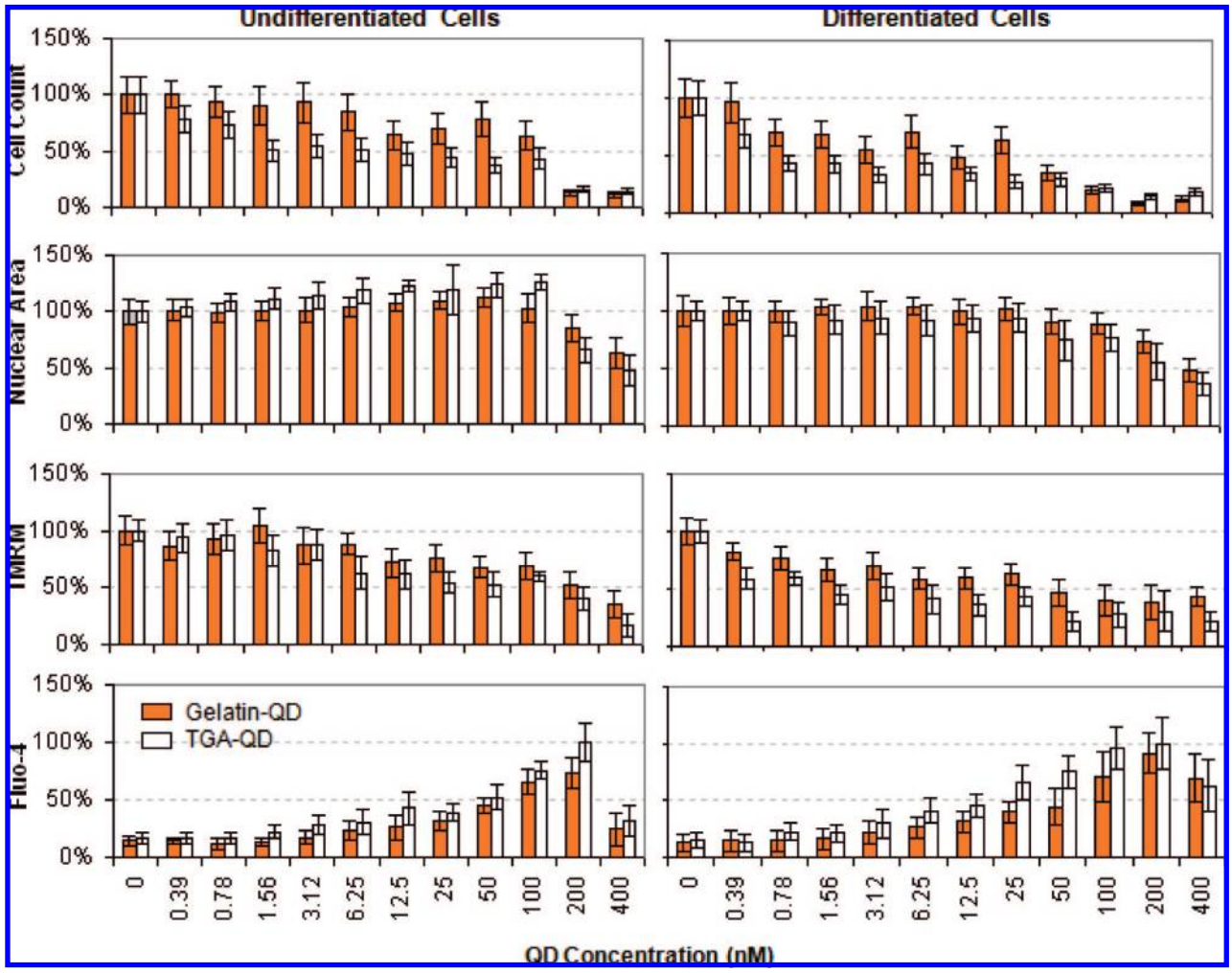

Figure 6. Cytotoxic effects of TGA-QDs (white bars) and Gelatin-QDs (gray bars) in NG108-15 cells. Undifferentiated (left half) and differentiated (right half) cells were treated with QDs for 24 h and assayed for cell number (Hoechst 33342; top), nuclear area (Hoechst 33342; second from top), mitochondrial membrane potential (TMRM; third from top), and intracellular ionized Ca (Fluo-4; bottom). At each concentration, five independent fields were imaged and analyzed. Data is expressed as average of three independent runs.

count for the higher sensitivity of differentiated neurons to cytotoxic substances.[46]

Gold Nanoparticles. As a final demonstration, we employed the multiplexed cytotoxicity assay to study the effect of gold NPs (Au NPs) on HepG2 human hepatocellular carcinoma cells. We have recently demonstrated the use of gold NPs for early detection of cancerous tumors and inflammatory responses by photoacoustic imaging.[22,47] Considering the numerous functionalization strategies available for Au NPs, the ability to characterize toxicity using a HCS platform will be immensely valuable for the development of biomedical applications. We chose the HepG2 cells because they are one of the most commonly used cell types for HCS studies and have implications for metal poisoning associated with hepatic toxicities.

TABLE 1. A Summary of the Onset of Change in Each of the Four Fluorescence Parameters

	onset of change			
	undifferentiated		differentiated	
fluorescence parameters	Gelatin-QD	TGA-QD	Gelatin-QD	TGA-QD
cell count (below 30%)	12.5 nM	1.56 nM	1.56 nM	0.39 nM
nuclear area (below 90%)	200 nM	200 nM	100 nM	50 nM
TMRM (below 70%)	50 nM	6.26 nM	6.25 nM	0.39 nM
Fluo-4 (above 30%)	25 nM	6.25 nM	12.6 nM	3.12 nM

Our study with Au NPs differs from those with CdTe QDs in a couple ways. In addition to the use of a different cell line, the Au NP study aims to determine the effect of exposure duration to the NPs, as well as postexposure changes in cell physiology, while the previous studies focus on the concentration-dependent effect of NPs. To investigate these effects, we treated HepG2 cells with Au NPs for various lengths of time (0, 1, 2, 4, and 6 h). Following the Au NP treatment, cells were washed with PBS and allowed to grow in fresh medium for an additional period of time (1, 2, and 4 days). Similar to the previous studies on NG108-15 cells, HepG2 cells were analyzed for nuclei count, nuclear area, mitochondrial membrane potential, and intracellular free calcium concentration by incubating with a

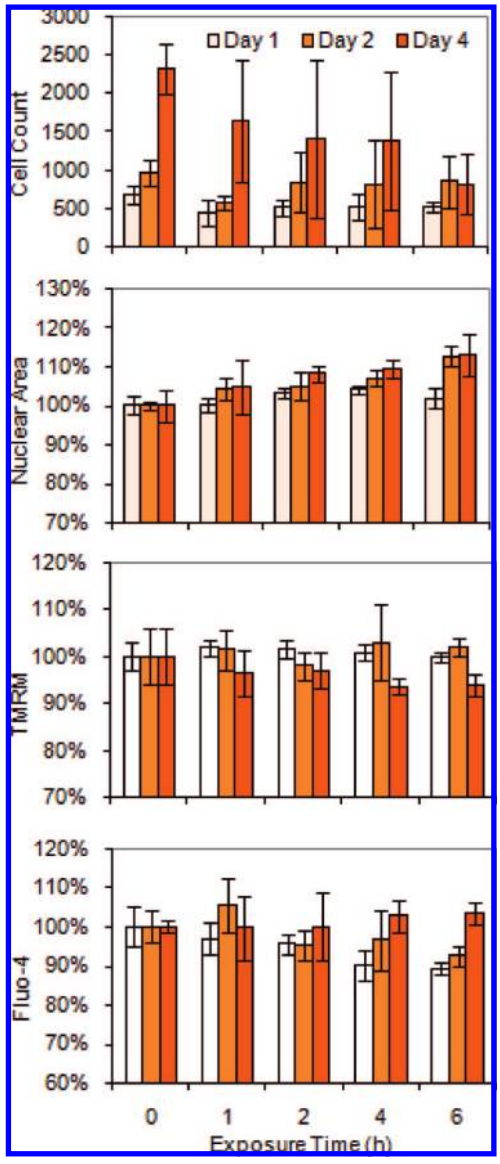

Figure 7. Cytotoxic effects of gold NPs in HepG2 cells. HepG2 cells were treated with gold NPs for 0, 1, 2, 4, and 6 h and assayed for cell number (Hoechst 33342; top), nuclear area (Hoechst 33342; second from top), mitochondrial membrane potential (TMRM; third from top), and intracellular ionized Ca (Fluo-4; bottom) 1, 2, and 4 days after treatment. Data is expressed as average of four independent runs.

cocktail of dye solutions and imaging with the IN Cell Analyzer 1000 HCS system to achieve complete fingerprinting of cellular response.

Our data suggest that Au NPs inhibited the proliferation of HepG2 cells. Figure 7 shows that although cell number appears to be relatively constant across different treatment times on day 1 and day 2 following Au NP treatment, it becomes inversely proportional to treatment time on day 4. Stronger inhibitory effect was observed with increasing exposure time to Au NPs. The inhibition of proliferation by Au NPs has been reported in other cells including endothelial cells and multiple myeloma cells.[48–50] Au NPs have been found to bind to and block the function of proteins that are essential for cell proliferation. In addition, Au NPs can also block and disrupt certain cellular signaling pathways that are required for growth and survival. In our study, this inhibitory effect was also accompanied by enlargement in the nuclear area. Cells having the longest exposure to Au NPs had an average nuclear area that was 13% larger than the untreated cells on day 4 after treatment. The concentration and exposure times of Au NPs employed in this study were shown to be only mildly cytotoxic to the HepG2 cells. Changes in the cellular mitochondrial membrane potential and intracellular free calcium concentration never deviated more than 10% from the untreated control. Treatment with Au NP reduced the mitochondrial membrane potential, which is a typical cellular response to cytotoxic material. The reduction was only apparent after 4 days following treatment and increased slightly with increasing exposure time. While cytotoxic stimulation typically leads to an increase in intracellular free calcium concentration, we unexpectedly observed a decrease in intracellular free calcium concentration 1 day following the Au NP treatment. The decrease appeared to be proportional to the exposure time, reaching approximately 10% for the longest exposed cells (6 h). Interestingly, the drop in intracellular free calcium concentration recovered by itself to the normal level as the culture time increased. The rate of recovery was inversely proportional to the exposure time, with the cells having the shortest exposure to Au NPs (1 h) making the quickest recovery. These findings indicate that the Au NPs inhibited intracellular calcium release in the HepG2 cells. Similar findings have also been reported for endothelial cells.[50] In our study, we also found this inhibitory effect by Au NPs to be reversible once the Au NPs are removed and the cells are allowed to recuperate in fresh medium.

CONCLUSION

In summary, we have demonstrated the use of various HCS assays to study the cytotoxicity of CdTe QDs and Au NPs in NG108-15 neuroblastoma cells and HepG2 human hepatocellular carcinoma cells. We found the neurite outgrowth assay, which assesses the functionality of differentiated neural cells, to be particularly important and the multiplexed cytotoxicity assay as a sensitive and informative assessment of toxicological mechanisms. The versatility of the multiplexed cytotoxicity assay was demonstrated across the different NPs tested in this study. The assays were capable of distinguishing the subtle differences in the cytotoxicity generated by TGA-QDs and Gelatin-QDs. The Gelatin-NPs, which are synthesized in the presence of gelatin, provide insight for surface modification and biofunctionalization of NPs. Most importantly, we demonstrated that undifferentiated and differentiated NG108-15 neuroblastoma cells respond differently to CdTe QD-induced cytotoxicity. Specifically, the differentiated

cells are more sensitive and vulnerable to QD treatment, which can be understood as the demonstration of adaptability of cells in undifferentiated state. This difference should be taken into account in the establishment of treatment dosage for any NP-based biological studies or therapies. Using the multiplexed cytotoxicity assay, we were able to uncover the inhibitory effect of Au NPs on cell growth and release of intracellular free calcium in HepG2 cells.

The cytotoxicity profiles generated from the multiplexed cytotoxicity assay can be regarded as the "fingerprints" of the corresponding nanomaterials. The multiparametric nature of these profiles will allow cytotoxicity analyses to be conducted at much higher throughput and accuracy in the future. The application of HCS technology in the study of nanomaterials is not limited to colloidal NPs and cytotoxicity studies, as we are in the progress of demonstrating its novel use on biocompatibility assessment of multilayer thin films produced from the LBL assembly. We are also exploring the use of HCS technology to study the transport and localization of engineered NPs in living cells. We believe this endeavor will help to shed light on the development of new drugs and drug delivery strategies based on nanomaterials.

We also consider it essential to mention here that the presented modality of the technique also has a significant limitation that needs to be addressed. It is related to the two-dimensional nature of cell cultures currently used in HCA most often. Cellular response in 2D cell cultures was shown to be different than cells in the natural tissue environment. More adequate 3D cell cultures techniques need to be developed. HCA does afford analysis of 3D images in a similar way as we presented here, however, the 3D approach will indeed require development of appropriate 3D matrixes (scaffolds), cell culture techniques, and refinement of software algorithms for image analysis. A suitable matrix must be transparent, mechanically robust, very biocompatible, and exceptionally standardized. Hydrogel matrixes made with geometry of inverted colloidal crystals[51,52] and potentially some others sharing the properties[53,54] mentioned above can be successfully used for this task.

METHODS

Synthesis of CdTe Quantum Dots. Thioglycolic acid (TGA)-capped CdTe QDs have been prepared according to published procedure.[55,56] Briefly, Millipore water (120 mL) was degassed by bubbling argon for approximately 1 h. $Cd(ClO_4)_2 \cdot 6H_2O$ (3.22 g, 7.68 mmol) and TGA stabilizer (1.24 g, 13.46 mmol, 1.75 mol equiv) were added, and the pH was adjusted to 11.2−11.3 by the addition of NaOH solution (2 M). For gelatin-containing samples, gelatin (0.3 g) was dissolved in water (10 mL) by heating gently and added to the reaction mixture. Gaseous H2Te, generated from Al_2Te_3 (0.56 g, 0.128 mmol) by dropwise addition of H_2SO_4 solution (0.5m) was bubbled through the cadmium/thiol/gelatin solution under a slow argon flow for approximately 10 min. The resultant nonluminescent solution was then heated to reflux. Fractions were precipitated by the addition of isopropanol and were stored at 4 °C.

Synthesis of Gold Nanoparticles. Gold chloride solution (0.01 g $HAuCl_4$ in 100 mL of water) was first brought to boil, followed by addition of 2 mL of 1% sodium citrate solution (0.02 g of trisodium citrate in 2 mL of water). The gold nanoparticle solution was stirred for 10 min and allowed to cool to room temperature. Stabilizer was introduced by adding 102 μL of cysteine solution (0.01 g of L-cysteine in 1 mL of water) to the gold nanoparticle solution with stirring. The final gold nanoparticle solution was filtered through a 0.22 μm filter for sterility and stored at room temperature.

Cell Culture. NG108-15 murine neuroblastoma × glioma hybrid cells and HepG2 Human hepatocyte carcinoma cells were obtained from the European Collection of Cell Cultures. NG108-15 cells were grown in high-glucose Dulbecco's modified Eagle's medium, supplemented with 10% (v/v) of fetal calf serum, 0.1 mM hypoxanthine, 1 μM aminopterin, and 16 μM thymidine. To induce differentiation, the amount of serum was lowered to 1% (v/v). HepG2 cells were cultured in Eagel minimum essential medium supplemented with 10% (v/v) fetal bovine serum.

Apoptosis/Necrosis Assay. Cells were seeded in a 96-well tissue culture plate (Nunc) and allowed to adhere overnight. At the indicated time point (1.5, 6, 24 h) following treatment with TGA-QDs or Gelatin-QDs, cells were stained with propidium iodide (1 μg/ml) and Hoechst 33342 (2 μg/ml) for 10 min at room temperature and imaged using the IN Cell Analyzer 1000 HCS system (GE Healthcare). The HCS system scans through the bottom of the plate, focuses on individual fields of cells, and acquires images at each selected fluorescence channel. Hoechst was visualized in the blue channel and propidium iodide in the red channel. The experiment was conducted in three independent runs. For each run, five independent fields from each well were imaged using a 20× objective. Cells were classified as either healthy, apopotic, or necrotic using the supervised classification function of the IN Cell Investigator image analysis software (GE Healthcare).

Neurite Outgrowth Assay. Cells were seeded in 96-well tissue culture plate and allowed to adhere overnight. After treatment with TGA-QDs or Gelatin-QDs for 6 h, cells were gently washed with fresh medium and cultured with reduced serum supplementation to induce neuronal differentiation. No supplementary growth factor was added. After 4 days of differentiation, cells were fixed in 2% paraformaldehyde, permeabilized in 0.1% Triton X-100 in 1% BSA, and stained using mouse anti-β-tubulin III (1:800 in 1% BSA; overnight at 4 °C) followed by Alexa Fluor 488 conjugated goat antimouse IgG (1:200; 1 h at 37 °C). The experiment was carried out in triplicate. For each well, four independent fields were imaged using a 10× objective and analyzed using the neurite outgrowth analysis module of the IN Cell Investigator software. The analysis module reports population-averaged measurements for a range of cell parameters, including neurite length and neurite count.

Multiplexed Cytotoxicity Assay. Cells were seeded in 96-well plate and allowed to adhere overnight. Following treatment with either CdTe QDs or Au NPs, cells were very gently washed with prewarmed fresh medium and simultaneously loaded with 1 μM Hoechst 33342, 20 nM TMRM (tetramethyl rhodamine methyl ester perchlorate), and 1 μM Fluo-4 (fluo-4 acetoxymethyl ester). Cells were loaded in the corresponding culture media for 30 min at 37 °C and then imaged using the IN Cell Analyzer 1000 HCS system. Hoechst was visualized in the blue channel while TMRM and Fluo-4 were visualized in the red and green channels, respectively. The following data were collected and analyzed using the dual area object analysis module of the IN Cell Investigator software. The module allows simultaneous quantification of subcellular inclusions that are marked by different fluorescent probes and measures fluorescence intensity associated with predefined nuclear and cytoplasmic compartments. The following

data were collected. Cell count was generated from the number of Hoechst 33342 stained nuclei. Nuclear size was defined as the mean object area of Hoechst 33342. Cellular mitochondrial membrane potential was measured by the TMRM fluorescence intensity in punctuate cytosolic regions (cellular inclusions) around the nucleus. Intracellular free calcium concentration was measured by the fluorescence intensity of Fluo-4 in an intracellular circular region (cellular compartment) centered at the nucleus.

Acknowledgment. N.A.K. thanks NIH, NSF, AFOSR, AFOSR-MURI, and Walton Fellowship from SFI for the support of this research.

REFERENCES AND NOTES

1. Zhang, Z. L.; Tang, Z. Y.; Kotov, N. A.; Glotzer, S. C. Simulations and Analysis of Self-Assembly of CdTe Nanoparticles into Wires and Sheets. *Nano Lett.* **2007**, *7*, 1670–1675.
2. Sarikaya, M.; Tamerler, C.; Jen, A. K. Y.; Schulten, K.; Baneyx, F. Molecular Biomimetics: Nanotechnology through Biology. *Nat. Mater.* **2003**, *2*, 577–585.
3. Tang, Z.; Zhang, Z.; Wang, Y.; Glotzer, S. C.; Kotov, N. A. Self-Assembly of CdTe Nanocrystals into Free-Floating Sheets. *Science (Washington, DC)* **2006**, *314*, 274–278.
4. Oberdorster, G.; Oberdorster, E.; Oberdorster, J. Nanotoxicology: An Emerging Discipline Evolving from Studies of Ultrafine Particles. *Environ. Health Perspect.* **2005**, *113*, 823–839.
5. Stone, V.; Donaldson, K. Nanotoxicology - Signs of Stress. *Nat. Nanotechnol.* **2006**, *1*, 23–24.
6. Donaldson, K.; Stone, V.; Tran, C. L.; Kreyling, W.; Borm, P. J. A. Nanotoxicology. *Occup. Environ. Med.* **2004**, *61*, 727–728.
7. Klostranec, J. M.; Chan, W. C. W. Quantum Dots in Biological and Biomedical Research: Recent Progress and Present Challenges. *Adv. Mater.* **2006**, *18*, 1953–1964.
8. Kirchner, C.; Liedl, T.; Kudera, S.; Pellegrino, T.; Javier, A. M.; Gaub, H. E.; Stolzle, S.; Fertig, N.; Parak, W. J. Cytotoxicity of Colloidal CdSe and CdSe/ZnS Nanoparticles. *Nano Lett.* **2005**, *5*, 331–338.
9. Derfus, A. M.; Chan, W. C. W.; Bhatia, S. N. Probing the Cytotoxicity of Semiconductor Quantum Dots. *Nano Lett.* **2004**, *4*, 11–18.
10. Hoshino, A.; Fujioka, K.; Oku, T.; Suga, M.; Sasaki, Y. F.; Ohta, T.; Yasuhara, M.; Suzuki, K.; Yamamoto, K. Physicochemical Properties and Cellular Toxicity of Nanocrystal Quantum Dots Depend on Their Surface Modification. *Nano Lett.* **2004**, *4*, 2163–2169.
11. Hardman, R. A Toxicologic Review of Quantum Dots: Toxicity Depends on Physicochemical and Environmental Factors. *Environ. Health Perspect.* **2006**, *114*, 165–172.
12. Giuliano, K. A.; Haskins, J. R.; Taylor, D. L. Advances in High Content Screening for Drug Discovery. *Assay Drug Dev. Technol.* **2003**, *1*, 565–577.
13. Comley, J. High Content Screening - Emerging Importance of Novel Reagents/Probes and Pathway Analysis. *Drug Discovery World* **2005**, 31–53.
14. Zhang, T. T.; Stilwell, J. L.; Gerion, D.; Ding, L. H.; Elboudwarej, O.; Cooke, P. A.; Gray, J. W.; Alivisatos, A. P.; Chen, F. F. Cellular Effect of High Doses of Silica-Coated Quantum Dot Profiled with High Throughput Gene Expression Analysis and High Content Cellomics Measurements. *Nano Lett.* **2006**, *6*, 800–808.
15. Michalet, X.; Pinaud, F. F.; Bentolila, L. A.; Tsay, J. M.; Doose, S.; Li, J. J.; Sundaresan, G.; Wu, A. M.; Gambhir, S. S.; Weiss, S. Quantum Dots for Live Cells, *In Vivo* Imaging, and Diagnostics. *Science (Washington, DC)* **2005**, *307*, 538–544.
16. Jaiswal, J. K.; Mattoussi, H.; Mauro, J. M.; Simon, S. M. Long-Term Multiple Color Imaging of Live Cells Using Quantum Dot Bioconjugates. *Nat. Biotechnol.* **2003**, *21*, 47–51.
17. Parak, W. J.; Gerion, D.; Pellegrino, T.; Zanchet, D.; Micheel, C.; Williams, S. C.; Boudreau, R.; Le Gros, M. A.; Larabell, C. A.; Alivisatos, A. P. Biological Applications of Colloidal Nanocrystals. *Nanotechnol.* **2003**, *14*, R15−R27.
18. Medintz, I. L.; Uyeda, H. T.; Goldman, E. R.; Mattoussi, H. Quantum Dot Bioconjugates for Imaging, Labelling and Sensing. *Nat. Mater.* **2005**, *4*, 435–446.
19. Thomas, M.; Klibanov, A. M. Conjugation to Gold Nanoparticles Enhances Polyethylenimine's Transfer of Plasmid DNA into Mammalian Cells. *Proc. Natl. Acad. Sci. U.S.A.* **2003**, *100*, 9138–9143.
20. Hirsch, L. R.; Stafford, R. J.; Bankson, J. A.; Sershen, S. R.; Rivera, B.; Price, R. E.; Hazle, J. D.; Halas, N. J.; West, J. L. Nanoshell-Mediated Near-Infrared Thermal Therapy of Tumors under Magnetic Resonance Guidance. *Proc. Natl. Acad. Sci. U.S.A.* **2003**, *100*, 13549–13554.
21. Chen, J.; Wiley, B.; Li, Z. Y.; Campbell, D.; Saeki, F.; Cang, H.; Au, L.; Lee, J.; Li, X.; Xia, Y. Gold Nanocages: Engineering Their Structure for Biomedical Applications. *Adv. Mater.* **2005**, *17*, 2255–2261.
22. Eghtedari, M.; Oraevsky, A.; Copland, J. A.; Kotov, N. A.; Conjusteau, A.; Motamedi, M. High Sensitivity of *In Vivo* Detection of Gold Nanorods Using a Laser Optoacoustic Imaging System. *Nano Lett.* **2007**, *7*, 1914–1918.
23. Copland, J. A.; Eghtedari, M.; Popov, V. L.; Kotov, N.; Mamedova, N.; Motamedi, M.; Oraevsky, A. A. Bioconjugated Gold Nanoparticles as a Molecular Based Contrast Agent: Implications for Imaging of Deep Tumors Using Optoacoustic Tomography. *Mol. Imaging Biol.* **2004**, *6*, 341–349.
24. Gomez, N.; Winter, J. O.; Shieh, F.; Saunders, A. E.; Korgel, B. A.; Schmidt, C. E. Challenges in Quantum Dot-Neuron Active Interfacing. *Talanta* **2005**, *67*, 462–471.
25. Pathak, S.; Cao, E.; Davidson, M. C.; Jin, S. H.; Silva, G. A. Quantum Dot Applications to Neuroscience: New Tools for Probing Neurons and Glia. *J. Neurosci.* **2006**, *26*, 1893–1895.
26. Vu, T. Q.; Maddipati, R.; Blute, T. A.; Nehilla, B. J.; Nusblat, L.; Desai, T. A. Peptide-Conjugated Quantum Dots Activate Neuronal Receptors and Initiate Downstream Signaling of Neurite Growth. *Nano Lett.* **2005**, *5*, 603–607.
27. Dahan, M.; Levi, S.; Luccardini, C.; Rostaing, P.; Riveau, B.; Triller, A. Diffusion Dynamics of Glycine Receptors Revealed by Single-Quantum Dot Tracking. *Science (Washington, DC)* **2003**, *302*, 442–445.
28. Jackson, H.; Muhammad, O.; Daneshvar, H.; Nelms, J.; Popescu, A.; Vogelbaum, M. A.; Bruchez, M.; Toms, S. A. Quantum Dots are Phagocytized by Macrophages and Colocalize with Experimental Gliomas. *Neurosurgery* **2007**, *60*, 524–529.
29. Winter, J. O.; Gomez, N.; Korgel, B. A.; Schmidt, C. E. In Quantum Dots for Electrical Stimulation of Neural Cells. *Proc. SPEI-Int. Soc. Opt. Eng.* **2005**, *5705*, 235–246. (Nanobiophotonics and Biomedical Applications II)
30. Winter, J. O.; Liu, T. Y.; Korgel, B. A.; Schmidt, C. E. Recognition Molecule Directed Interfacing between Semiconductor Quantum Dots and Nerve Cells. *Adv. Mater.* **2001**, *13*, 1673–1677.
31. Pappas, T. C.; Wickramanyake, W. M. S.; Jan, E.; Motamedi, M.; Brodwick, M.; Kotov, N. A. Nanoscale Engineering of a Cellular Interface with Semiconductor Nanoparticle Films for Photoelectric Stimulation of Neurons. *Nano Lett.* **2007**, *7*, 513–519.
32. Byrne, S. J.; Williams, Y.; Davies, A.; Corr, S. A.; Rakovich, A.; Gun'ko, Y. K.; Rakovich, Y. P.; Donegan, J. F.; Volkov, Y. "Jelly Dots": Synthesis and Cytotoxicity Studies of CdTe Quantum Dot-Gelatin Nanocomposites. *Small* **2007**, *3*, 1152–1156.
33. Chan, W. H.; Shiao, N. H.; Lu, P. Z. CdSe Quantum Dots Induce Apoptosis in Human Neuroblastoma Cells via Mitochondrial-Dependent Pathways and Inhibition of Survival Signals. *Toxicol. Lett.* **2006**, *167*, 191–200.
34. Calabrese, E. J.; Baldwin, L. A. Applications of Hormesis in Toxicology, Risk Assessment and Chemotherapeutics. *Trends Pharmacol. Sci.* **2002**, *23*, 331–337.
35. O'Brien, P. J.; Irwin, W.; Diaz, D.; Howard-Cofield, E.; Krejsa, C. M.; Slaughter, M. R.; Gao, B.; Kaludercic, N.; Angeline, A.; Bernardi, P.; Brain, P.; Hougham, C. High Concordance of Drug-Induced Human Hepatotoxicity with *In Vitro*

Cytotoxicity Measured in a Novel Cell-Based Model using High Content Screening. *Arch. Toxicol.* **2006**, *80*, 580–604.
36. Xu, J. J.; Diaz, D.; O'Brien, P. J. Applications of Cytotoxicity Assays and Pre-lethal Mechanistic Assays for Assessment of Human Pepatotoxicity Potential. *Chem.-Biol. Interact.* **2004**, *150*, 115–128.
37. Plymale, D. R.; Haskins, J. R.; Iglesia, F. A. d. l. Monitoring Simultaneous Subcellular Events In Vitro by Means of Coherent Multiprobe Fluorescence. *Nat. Med. (N.Y.)* **1999**, *5*, 351–355.
38. Kann, O.; Kovacs, R. Mitochondria and Neuronal Activity. *Am. J. Physiol. Cell Physiol.* **2007**, *292*, C641−657.
39. Nicholls, D. G. Mitochondrial Membrane Potential and Aging. *Aging Cell* **2004**, *3*, 35–40.
40. Orrenius, S.; Nicotera, P. The Calcium-Ion and Cell-Death. *J. Neural Transm. Suppl.* **1994**, 1–11.
41. Monteith, G. R.; Bird, G. S. J. Techniques: High-Throughput Measurement of Intracellular Ca2+−Back to Basics. *Trends Pharmacol. Sci.* **2005**, *26*, 218–223.
42. Mattson, M. P. Calcium and Neurodegeneration. *Aging Cell* **2007**, *6*, 337–350.
43. Chin, T.-Y.; Hwang, H.-M.; Chueh, S.-H. Distinct Effects of Different Calcium-Mobilizing Agents on Cell Death in NG108-15 Neuroblastoma X Glioma Cells. *Mol. Pharmacol.* **2002**, *61*, 486–494.
44. Orrenius, S.; McCabe, M. J.; Nicotera, P. Ca2+-Dependent Mechanisms of Cytotoxicity and Programmed Cell Death. *Toxicol. Lett.* **1992**, *64−65*, 357–364.
45. Zornetzer, M. S.; Stein, G. S. Gene Expression in Mouse Neuroblastoma Cells: Properties of the Genome. *Proc. Natl. Acad. Sci. U.S.A.* **1975**, *72*, 3119–3123.
46. Clarkson, E. D.; Edwards-Prasad, J.; Freed, C. R.; Prasad, K. N. Immortalized Dopamine Neurons: A Model to Study Neurotoxicity and Neuroprotection. *Proc. Soc. Exp. Biol. Med.* **1999**, *222*, 157–163.
47. Kim, K.; Huang, S. W.; Ashkenazi, S.; O'Donnell, M.; Agarwal, A.; Kotov, N. A.; Denny, M. F.; Kaplan, M. J. Photoacoustic Imaging of Early Inflammatory Response Using Gold Nanorods. *Appl. Phys. Lett.* **2007**, *90*, 223901.
48. Bhattacharya, R.; Mukherjee, P.; Xiong, Z.; Atala, A.; Soker, S.; Mukhopadhyay, D. Gold Nanoparticles Inhibit VEGF165-Induced Proliferation of HUVEC Cells. *Nano Lett.* **2004**, *4*, 2479–2481.
49. Bhattacharya, R.; Patra, C. R.; Verma, R.; Kumar, S.; Greipp, P. R.; Mukherjee, P. Gold Nanoparticles Inhibit the Proliferation of Multiple Myeloma Cells. *Adv. Mater.* **2007**, *19*, 711–716.
50. Mukherjee, P.; Bhattacharya, R.; Wang, P.; Wang, L.; Basu, S.; Nagy, J. A.; Atala, A.; Mukhopadhyay, D.; Soker, S. Antiangiogenic Properties of Gold Nanoparticles. *Clin. Cancer Res.* **2005**, *11*, 3530–3534.
51. Kotov, N. A. Inverted Colloidal Crystals as Three-Dimensional Cell Scaffolds. *Langmuir* **2004**, *20*, 7887–7892.
52. Lee, J.; Lee, J. Inverted Colloidal Crystals as Three-Dimensional Microenvironments for Cellular Co-Cultures. *J. Mater. Chem.* **2006**, *16*, 3558–3564.
53. Yokoi, H.; Kinoshita, T.; Zhang, S. Dynamic Reassembly of Peptide RADA16 Nanofiber Scaffold. *Proc. Natl. Acad. Sci. U.S.A.* **2005**, *102*, 8414–8419.
54. Stachowiak, A. N.; Bershteyn, A.; Tzatzalos, E.; Irvine, D. J. Bioactive Hydrogels with an Ordered Cellular Structure Combine Interconnected Macroporosity and Robust Mechanical Properties. *Adv. Mater.* **2005**, *17*, 399–403.
55. Gaponik, N.; Talapin, D. V.; Rogach, A. L.; Hoppe, K.; Shevchenko, E. V.; Kornowski, A.; Eychmuller, A.; Weller, H. *J. Phys. Chem. B* **2002**, *106*, 7177–7185.
56. Byrne, S. J.; Corr, S. A.; Rakovich, T. Y.; Gun'ko, Y. K.; Rakovich, Y. P.; Donegan, J. F.; Mitchell, S.; Volkov, Y. *J. Mater. Chem.* **2006**, *16*, 2896–2902.